Chinese Chemical Letters 36 (2025) 109729

Contents lists available at ScienceDirect

Chinese Chemical Letters

journal homepage: www.elsevier.com/locate/cclet

Enhancing ethane/ethylene separation performance through the amino-functionalization of ethane-selective MOF

Yao-Yu Ma, Wen-Juan Shi*, Gang-Ding Wang, Xin Liu, Lei Hou*, Yao-Yu Wang

Key Laboratory of Synthetic and Natural Functional Molecule of the Ministry of Education, Shaanxi Key Laboratory of Physico-Inorganic Chemistry, College of Chemistry & Materials Science, Northwest University, Xi'an 710069, China

ARTICLE INFO

Article history:
Received 26 December 2023
Revised 29 January 2024
Accepted 23 February 2024
Available online 9 March 2024

Keywords:
Metal-organic framework
Amino-functionalization
Gas adsorption
Adsorption selectivity
Separation

ABSTRACT

The utilization of ethane-selective materials for adsorption-based separation technology presents an energy-efficient alternative to cryogenic distillation for ethylene (C_2H_4) purification from ethane (C_2H_6). To study the relations between separation performance and pore environments, we carried out the isoreticular chemistry rule to introduce the -NH_2 groups into a C_2H_6-selective MOF [$Cu_{1.5}$(BTC)(DPU)$_{1.5}$(H_2O)$_{1.5}$], and successfully improved the adsorption capacity and selectivity for C_2H_6 over C_2H_4. The NH_2-functionalized MOF [$Cu_{1.5}$(NH_2-BTC)(DPU)$_{1.5}$(H_2O)$_{1.5}$] with a relatively narrow pore not only forms appropriate pore restriction but also provides additional binding sites to enhance the adsorption capacity of C_2H_6 relative to C_2H_4. Both gas adsorption and dynamic breakthrough results indicated that the -NH_2 functionalization significantly enhanced the separation performance of materials for C_2H_6/C_2H_4 mixtures, allowing the production of C_2H_4 with a purity of over 99.99% and a productivity of up to 30.02 L/kg in one step. Theoretical calculations revealed that the synergistic effect of appropriate pore confinement and NH_2-modified functional surfaces imposed stronger interactions on C_2H_6 than C_2H_4.

Ethylene (C_2H_4), as one of the world's largest chemical products, is the core of the petrochemical industry. Currently, a majority of the world's C_2H_4 is produced by thermal cracking of ethane (C_2H_6) or steam cracking, and C_2H_6 is inevitably existed as a major byproduct [1]. The separation of C_2H_6 from C_2H_4 is thereby a critical process to yield polymer-grade C_2H_4 (>99.9%) for polymer production [2]. The industrial separation of C_2H_4 from C_2H_6 typically relies on high-pressure cryogenic distillation at temperatures as low as −160 °C because of the similar sizes and volatilities between them, representing one of the most energy-intensive processes [3]. Hence, the energy-efficient separation technology for the production of polymer grade C_2H_4 is highly desired and challenging [4].

Separation by means of adsorption using porous materials is recognized as a promising alternative because of low energy consumption and high efficiency [5–11]. Metal-organic frameworks (MOFs) are porous crystalline materials formed by self-assembly of inorganic metal centers with organic ligands. In comparison to traditional porous materials, MOFs are regarded as excellent C_2H_6/C_2H_4 separation and purification platforms owing to their ability to accurately adjust the framework structures and functionalize the pore surfaces. MOFs for C_2H_6/C_2H_4 separation were divided into C_2H_4-selective MOFs and C_2H_6-selective MOFs [12–17]. In general, the design of C_2H_4-selective MOFs is easier to implement through taking advantage of stronger interactions between unsaturated C_2H_4 molecules and high polar binding centers, such as open metal sites. However, to get C_2H_4 product, the next desorption process is necessary, which is still difficult to produce highly pure C_2H_4 due to co-adsorption of C_2H_6 in materials, so it needs the multiple adsorption-desorption cycles and is also energetically costly [18–23]. On the contrary, C_2H_6-selective MOFs can preferentially capture C_2H_6 impurity to directly produce C_2H_4 at the separation column outlet [24–28], which is more facile and economical process, and can also greatly reduce energy consumption [29]. But C_2H_6-selective MOFs usually exhibit relatively low loading or selectivity due to lacking strong binding sites. So it is imperative to develop new C_2H_6-selective MOFs for efficient C_2H_4 purity [30–35].

The challenge of separating C_2H_6 and C_2H_4 stems from their very close molecular sizes and boiling points (Table S1 in Supporting information) [36]. Compared to C_2H_4, C_2H_6 has a smaller quadrupole moment (0.65×10^{-26} esu cm^2 *vs.* 1.50×10^{-26} esu cm^2) and a larger polarizability (44.7×10^{-25} cm^3 *vs.* 42.52×10^{-25}

* Corresponding authors.
E-mail addresses: swjuan2000@126.com (W.-J. Shi), lhou2009@nwu.edu.cn (L. Hou).

https://doi.org/10.1016/j.cclet.2024.109729
1001-8417/

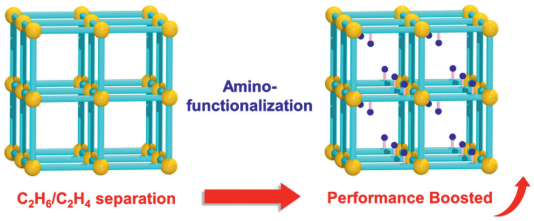

Scheme 1. Strategy to boost C_2H_6/C_2H_4 separation through pore functionalization.

cm^3), indicating that dispersion and induction interactions would make major contributions in C_2H_6-selective adsorbents [37]. C_2H_6-selective MOFs can be obtained by designing inert pore surfaces or implanting C_2H_6 affinity sites which will preferentially adsorb C_2H_6 over C_2H_4 [17,24,38-42]. For example, Chen *et al.* reported a microporous MOF, $Fe_2(O_2)$(dobdc), with iron (Fe)-peroxo sites for preferential binding of C_2H_6 over C_2H_4, showing a separation selectivity of up to 4.4 for C_2H_6/C_2H_4 [24]. By virtue of pore engineering, Li *et al.* successfully designed an inert ultramicroporous material ($Cu(Qc)_2$) with optimized pore structure, realizing excellent C_2H_6-selective adsorption behavior [39]. Although some C_2H_6-selective MOFs have been reported, there are still some deficiencies such as typical "trade-off" effect between selectivity and capacity, balancing these issues remains a constant challenge [43].

The adsorption amounts and selectivity for gases in MOFs are crucial for separation, which are closely dependent on the pore environments of MOFs. Therefore, the regulation of pore walls through using functionalized ligands would provide an important approach to enhance the separation performance of MOFs for C_2H_6/C_2H_4 mixtures (Scheme 1). To target MOFs with the preferential binding of C_2H_6 over C_2H_4, we initially designed a C_2H_6-selective MOF [$Cu_{1.5}$(BTC)$(DPU)_{1.5}(H_2O)_{1.5}$] (Cu-MOF) from 1,3,5-benzenetricarboxylic acid (H_3BTC) and 1,3-di(pyridin-4-yl)urea (DPU) linkers, which possesses abundant urea groups in pores and will provide stronger multiple interactions with C_2H_6 over C_2H_4. Then according to the isoreticular principle, the -NH_2 groups that could be the potential adsorption sites through hydrogen bonds with gas molecules were embedded into the pores through replacing H_3BTC with NH_2-H_3BTC ligands, generating the isomorphic framework Cu-MOF(NH_2), [$Cu_{1.5}$(NH_2-BTC)$(DPU)_{1.5}(H_2O)_{1.5}$], with more accessible sites in pores to study the control of pore chemistry for advancing C_2H_6/C_2H_4 separation. It was found that due to the electronegative N/O sites and the coordination between water and metal centers hindering the open metal sites (OMSs), both MOFs exhibited C_2H_6-selective adsorption behaviors. In particular, the introduction of -NH_2 groups in pores provides additional binding sites to more enhance the binding affinity for C_2H_6, leading to increased C_2H_6 and C_2H_4 uptakes and C_2H_6/C_2H_4 selectivity (from 1.4 to 1.8) in Cu-MOF(NH_2) compared to Cu-MOF. The breakthrough experiments also showed that Cu-MOF(NH_2) can obtain highly pure C_2H_4 (≥99.99%) in one step with longer breakthrough interval times and higher C_2H_4 productivity.

The synthesis details of Cu-MOF and Cu-MOF(NH_2) were given in Supporting information. Single-crystal X-ray diffraction analysis determined that two MOFs exhibited isomorphic network and crystallized in the same trigonal crystal system (Tables S2 and S3 in Supporting information). The crystal structure of NH_2-functionalized Cu-MOF(NH_2) was described representatively. The asymmetric unit contains half a Cu^{2+} ion, half a DPU ligand, two-thirds of deprotonated NH_2-BTC ligand, and half a H_2O coordinated molecule. The Cu^{2+} ion has a distorted square pyramidal geometry constituted by two carboxylate O atoms from two NH_2-BTC and two pyridine N atoms from two DPU on the base plane and one water O atom on the vertex (Fig. 1a). Six Cu^{2+} ions and six NH_2-BTC are alternately connected to form a 48-membered planar

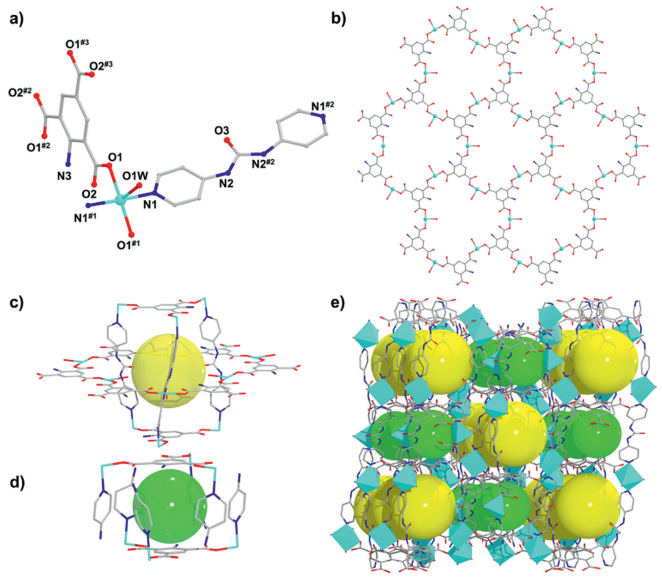

Fig. 1. (a) Coordination environment of Cu^{2+} ion, (b) layer, (c) cage I, (d) cage II, and (e) 3D framework in Cu-MOF(NH_2).

ring, which extends outward to form a layer with hexagonal windows (Fig. 1b). Furthermore, the linkages of adjacent layers with DPU as pillars to afford a (3,4)-connected three-dimensional network, which with large windows is threaded by the other network to afford a two-folded interpenetrated framework. The upper and lower BTC–Cu coordinated motifs in an independent network are supported by three DPU pillars to form a triangular prism-like cage (cage I), and which passes through one ring in the layer of the other network to form a cavity with six windows (Fig. 1c). Along the *c* axis, the other cage (cage II) (Fig. 1d) is also formed between two independent networks on both sides of cage I. These cavities are connected to form channels with abundant accessible N/O sites (Fig. 1e), in particular the modification of -NH_2 groups in Cu-MOF(NH_2) provides more potential sites in channels compared to Cu-MOF, which may play a positive role in enhancing the separation performance for C_2H_6/C_2H_4 mixtures.

Sample purity was verified by matched powder X-ray diffraction (PXRD) between the measured results of as-synthesized samples and the simulated patterns from single crystal structures (Figs. S1 and S2 in Supporting information). Thermogravimetric analysis (TGA) indicated the initial weight loss of lattice solvent molecules in two MOFs before 110 °C. After a thermal stable platform, the skeleton began to decompose at 250 °C (Figs. S3 and S4 in Supporting information). Fourier transform infrared spectrum (FT-IR) peaks of Cu-MOF(NH_2) at 3306 and 3400 cm^{-1} are the characteristic peaks of N–H vibration from -NH_2 groups, however, Cu-MOF only possessed one peak at 3307 cm^{-1} (Figs. S5 and S6 in Supporting information). Meanwhile, Cu-MOF(NH_2) also showed the peak at 1379 cm^{-1}, resulted from the C–N bond between the benzene ring and the amino group (Fig. S6 in Supporting information) [44]. The frameworks of two MOFs were activated by heating at 110 °C under vacuum for 3 h for the acetone-exchanged (72 h) samples. It can be found that the coordinated water molecules which correspond to the initial weight loss in activated samples were held (Figs. S3 and S4 in Supporting information). The coordination water molecules exclude the exposed metal ions which are not favorable for C_2H_6 selectivity over C_2H_4.

The identical frameworks but different potential adsorption sites between two MOFs provide good platforms for studying the influence of pore environments on gas separation. Two MOFs revealed type-I N_2 adsorption isotherms with the close loadings of

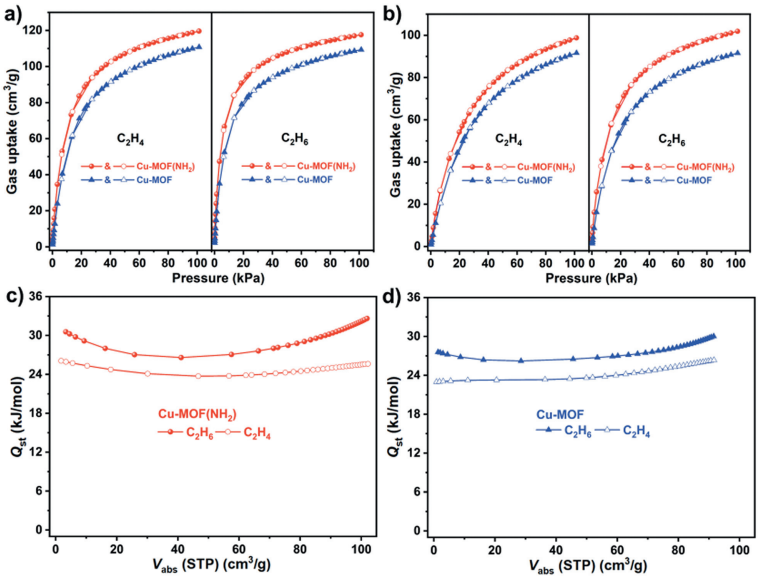

Fig. 2. Gas adsorption isotherms of Cu-MOF and Cu-MOF(NH_2) at (a) 273 and (b) 298 K. Q_{st} plots of (c) Cu-MOF(NH_2) and (d) Cu-MOF.

about 280 cm^3/g at 77 K and 100 kPa as well as the pore sizes of 6.5–8.5 Å (Figs. S7 and S8 in Supporting information). To evaluate the adjustment on C_2H_6/C_2H_4 separation by -NH_2 modification, single-component adsorption isotherms were measured. As shown in Figs. 2a and b, the uptakes of Cu-MOF for C_2H_4 and C_2H_6 at 100 kPa are 110.8 and 109.3 cm^3/g at 273 K and 91.6 and 91.5 cm^3/g at 298 K, respectively, however, those valves in Cu-MOF(NH_2) are increased to 119.6 and 117.6 cm^3/g at 273 K and 98.8 and 101.3 cm^3/g at 298 K, respectively. At the same time, the adsorption isotherms of Cu-MOF(NH_2) are moderately steeper than Cu-MOF, indicating that the pore modification by -NH_2 groups makes an increase in adsorption for two gases. Further, the isosteric heat of adsorption (Q_{st}) was calculated by fitting adsorption isotherms to virial equation, which revealed the affinity of MOFs toward adsorbates (Figs. S9-S12 in Supporting information). As shown in Figs. 2c and d, the initial Q_{st} values for C_2H_6 of 30.6 kJ/mol in Cu-MOF(NH_2) and 27.6 kJ/mol in Cu-MOF are higher than the corresponding values for C_2H_4 of 26.1 and 23.0 kJ/mol, indicating stronger interactions of two MOFs for C_2H_6. Meanwhile, the slopes of C_2H_6 isotherms are also significantly larger than those of C_2H_4. These results illustrated a stronger affinity of the framework for C_2H_6 than C_2H_4, supporting the C_2H_6-selective behavior in two MOFs. In addition, the adsorption cyclic tests of Cu-MOF(NH_2) showed repeated results with no decrease in adsorption capacity (Fig. S13 in Supporting information).

After surveying the improvement of C_2H_6-selective adsorption and higher C_2H_6-binding affinity in Cu-MOF(NH_2), ideal adsorbed solution theory (IAST) was utilized to calculate the adsorption selectivity of Cu-MOF(NH_2) for 1/1, 1/9, and 1/15 of C_2H_6/C_2H_4 mixtures and compared to those of Cu-MOF (Figs. S14-S17 in Supporting information). As shown in Fig. 3a, Cu-MOF(NH_2) exhibits the C_2H_6/C_2H_4 selectivity of about 1.8 for equimolar mixtures at 298 K and 100 kPa, which is significantly higher than that of Cu-MOF (1.4), and is equivalent to some top-performing C_2H_6-selective materials, such as CPM-733 (1.75) [45], ZIF-8 (1.7) [46], PCN-250 (1.9) [47], and Zn-atz-ipa (1.7) [40], but greatly surpasses some excellent MOFs, including TJT-100(1.2) [30], Azole-Th-1 (1.46) [25], UPC-612 (1.4) [26], and Ni(bdc)(ted)$_{0.5}$ (1.6) [48]. We used the separation potential (Δq) as a further evaluation and screening metric of MOFs [49]. As shown in Fig. 3b, Figs. S18 and S19 (Supporting information), the pure amounts of C_2H_4 recovered from Cu-MOF are 0.66, 1.40, and 1.49 mmol/g for the 1/1, 1/9, and 1/15 mixtures, respectively, however which are greatly increased to 1.24, 2.95, and 3.17 mmol/g for Cu-MOF(NH_2). In addition, taking the 1/15 mixtures as an example, the Δq of Cu-MOF(NH_2) are higher than many benchmark C_2H_6-selective materials, including MUF-15 (2.97 mmolg) [31], UiO-67-(NH_2)$_2$ (2.51 mmol/g) [50], and Cu(Qc)$_2$ (1.73 mmol/g) [39], thus outperforming many reported adsorbents [17,42,47].

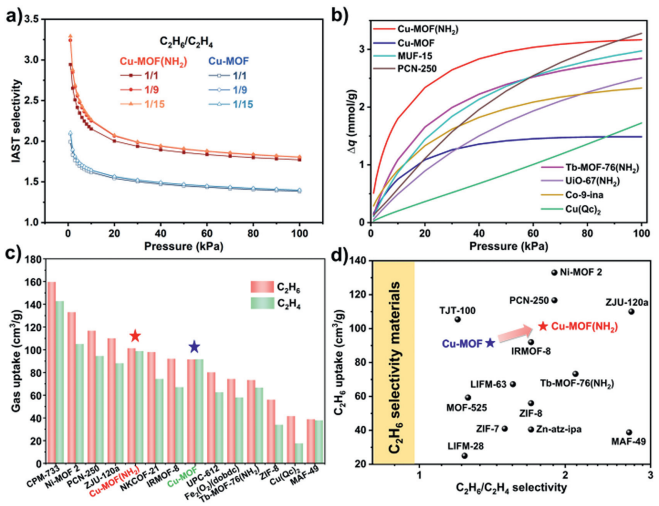

Fig. 3. (a) IAST selectivity of Cu-MOF and Cu-MOF(NH_2) for C_2H_6/C_2H_4 mixtures. (b) Separation potential for C_2H_6/C_2H_4 mixtures (1/15) in different materials. (c) Comparison of C_2H_4 and C_2H_6 uptakes in different materials. (d) Comparison of C_2H_6 uptakes and C_2H_6/C_2H_4 selectivity in different materials.

Adsorption amount is as equally important as the selectivity, however, due to frequently existed "trade-off" effect between selectivity and adsorption amount for separation in MOFs, it is challenging to simultaneously achieve both high C_2H_6/C_2H_4 selectivity and high C_2H_6 loading in one MOF. Although the C_2H_6 uptake of Cu-MOF(NH_2) (101.3 cm^3/g) is not as good as several prominent MOFs, such as CPM-733 (159.6 cm^3/g) [45], Ni-MOF 2 (133 cm^3/g) [35], PCN-250 (116.7 cm^3/g) [47], and ZJU-120a (110 cm^3/g) [33], based on different pore environments and framework topologies, but is greatly higher than most reported MOFs, such as MAF-49 (38.8 cm^3/g) [38], Cu(Qc)$_2$ (41.5 cm^3/g) [39], ZIF-8 (56 cm^3/g)

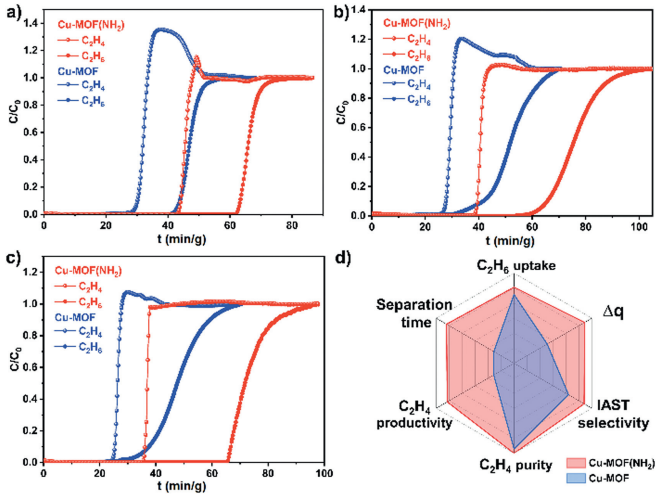

Fig. 4. Breakthrough curves of MOFs for C_2H_6/C_2H_4 mixtures at 298 K, (a) 1/1, (b) 1/9, and (c) 1/15. (d) Comparison of the comprehensive separation performance for Cu-MOF(NH_2) and Cu-MOF.

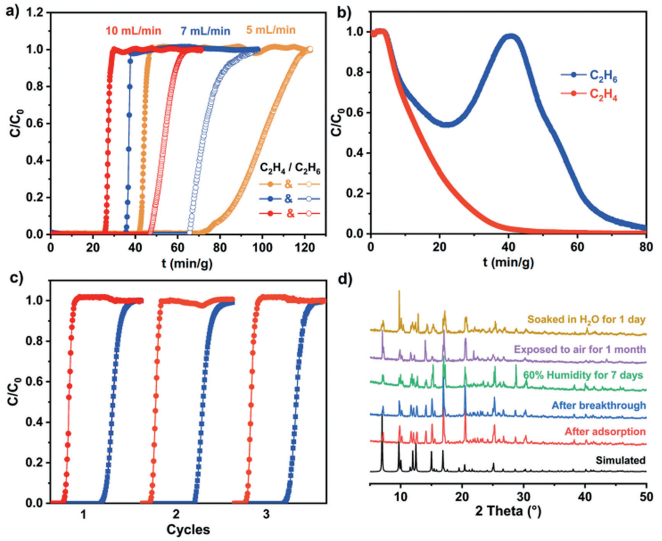

Fig. 5. (a) Breakthrough curves of Cu-MOF(NH_2) for C_2H_6/C_2H_4 (v/v, 1/15) mixtures at different total flow rates at 298 K. (b) Desorption curves of Cu-MOF(NH_2) for C_2H_6/C_2H_4 (v/v, 1/15) mixtures under Ar (7 mL/min) weeping at 323 K. (c) Breakthrough cycles of Cu-MOF(NH_2) for C_2H_6/C_2H_4 mixtures (v/v, 5/5) at 298 K. (d) PXRD patterns of Cu-MOF(NH_2) treated with different environments.

[46], $Fe_2(O_2)$(dobdc) (74.3 cm^3/g) [24], and UPC-612 (80.1 cm^3/g) (Fig. 3c) [26]. Taken together, Cu-MOF(NH_2) not only exhibits good C_2H_6/C_2H_4 selectivity but also excellent C_2H_6 uptake, signifying the potential as an efficient material for one-step purity of C_2H_4 from C_2H_6/C_2H_4 mixtures (Fig. 3d).

To further evaluate the effect of -NH_2 groups on C_2H_6/C_2H_4 separation performance, dynamic breakthrough experiments were conducted in a packed column filled with activated MOFs for C_2H_6/C_2H_4/Ar (5/5/90, 1/9/90, and 1/15/84, v/v/v, flow rate = 7.0 mL/min, Ar as carrier gas) mixtures at 298 K and 100 kPa, respectively. As shown in Fig. 4, two MOFs can separate C_2H_6/C_2H_4 mixtures, whereby Cu-MOF(NH_2) presents a considerably superior performance compared to Cu-MOF, aligning with the predicted results based on gas adsorption amount and IAST selectivity. As shown in Fig. 4a, C_2H_6 can be effectively separated from C_2H_6/C_2H_4 (50/50) mixtures in Cu-MOF, in which a high-purity C_2H_4 (≥99.9%) of 3.77 L/kg productivity is obtained at the outlet. However, Cu-MOF is failed to efficiently eliminate C_2H_6 from 1/9 and 1/15 C_2H_6/C_2H_4 mixtures because of low selectivity for C_2H_6 over C_2H_4, which leads to negligible C_2H_4 productivity and short separation time (Figs. 4b and c). By contrast, for Cu-MOF(NH_2), the ≥99.99% purity of C_2H_4 with 5.81, 8.33, and 30.02 L/kg productivity can be directly recovered from the 1/1, 1/9, and 1/15 C_2H_6/C_2H_4 mixtures in one cycle, respectively. The higher C_2H_4 productivity and longer breakthrough interval times determined by breakthrough experiments indicated that the immobilization of -NH_2 groups in MOF successfully optimized pore confinement, which associated with additional binding sites significantly improved the separation of material for C_2H_6/C_2H_4 mixtures (Fig. 4d). Considering better separation performance of Cu-MOF(NH_2), the breakthrough measurements at different flow rates of C_2H_6/C_2H_4 mixtures (1/15, v/v) were further conducted at 298 K in Cu-MOF(NH_2), it also indicated the complete separation of C_2H_6/C_2H_4 mixtures (Fig. 5a). Notably, as shown in Fig. 5b, Cu-MOF(NH_2) can also be easily regenerated by purging with Ar at 323 K, in which the adsorbed C_2H_4 due to weaker binding affinity is desorbed more quickly than C_2H_6. The breakthrough experiment cycles were performed on equimolar C_2H_6/C_2H_4 mixtures to investigate the reproducibility and recyclability of Cu-MOF(NH_2), which showed no decrease in separation performance (Fig. 5c). In addition, the PXRD measurements revealed that the framework treated with different environments retained structural integrity with no phase change and loss of crystallinity observed (Fig. 5d).

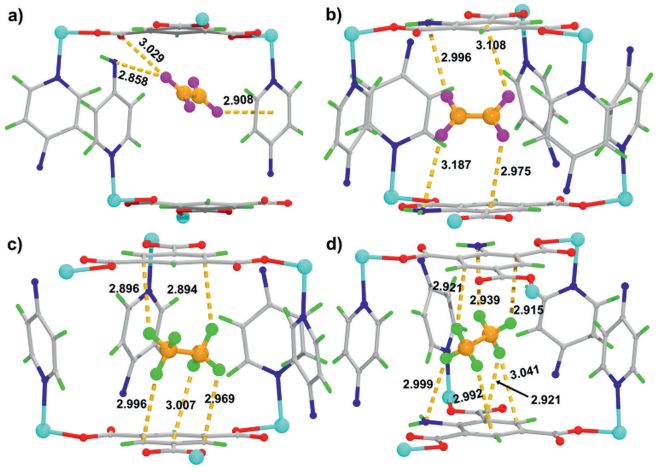

Fig. 6. (a, b) C_2H_4 and (c, d) C_2H_6 preferential adsorption sites in Cu-MOF and Cu-MOF(NH_2).

To in-depth elucidate the origin of C_2H_6-selective behavior enhanced by -NH_2 functionalization, grand canonical Monte Carlo (GCMC) simulations were done to investigate the interactions between the frameworks and gas molecules. As shown in Figs. 6a and b, in Cu-MOF the preferential adsorption sites for C_2H_4 and C_2H_6 are located in cages I and II, respectively. The C_2H_4 molecule interacts with one pyridine ring and one urea N atom from DPU, and one carboxylate O atom from BTC, through C–H···π and C–H···N/O interactions. By contrast, the C_2H_6 molecule is resided between two BTC linkers and involved in more hydrogen bonds and C–H···π interactions with the phenyl rings. For Cu-MOF(NH_2), the preferential adsorption sites for C_2H_6 and C_2H_4 are both located in cage II (Figs. 6c and d). The C_2H_4 molecule forms two C–H···N hydrogen bonds and two C–H···π interactions with the -NH_2 groups and phenyl rings in the upper and lower NH_2-BTC ligands, while the C_2H_6 molecule interacts with two phenyl rings from two NH_2-BTC through forming four C–H···C and one C–H···π interactions with the distances of 2.915–3.041 Å, as well as two stronger C–H···N (H···N = 2.939 and 2.999 Å) interactions compared to C_2H_4 (H···N = 2.996 and 3.187 Å). Therefore, the introduction of -NH_2

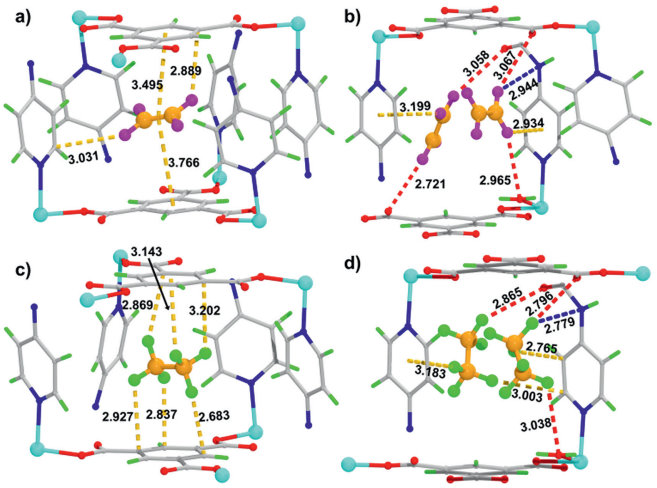

Fig. 7. (a, b) C_2H_4 and (c, d) C_2H_6 adsorption sites at 298 K and 100 kPa in Cu-MOF.

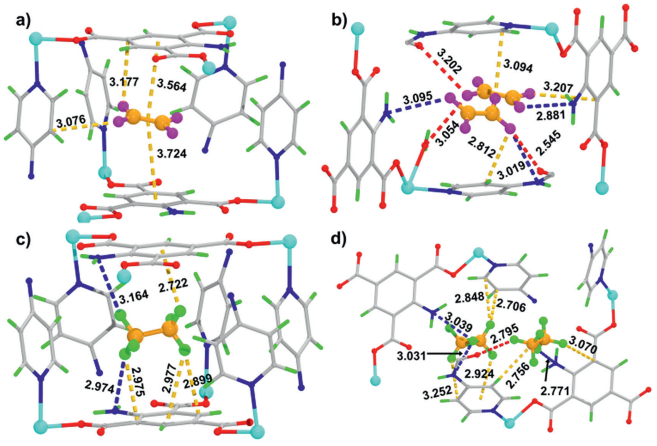

Fig. 8. (a, b) C_2H_4 and (c, d) C_2H_6 adsorption sites at 298 K and 100 kPa in Cu-MOF(NH_2).

groups not only changes the position of preferential adsorption sites, but also makes C_2H_4 and C_2H_6 molecules more closely contact with the pore walls. In particular, there obviously exist more supramolecular contacts between C_2H_6 molecule and pore walls in Cu-MOF(NH_2). Meanwhile, the calculated binding energies for C_2H_6 and C_2H_4 in Cu-MOF(NH_2) (42.5 kJ/mol *vs.* 32.3 kJ/mol) also showed the higher values compared to Cu-MOF (37.5 kJ/mol *vs.* 29.4 kJ/mol). These findings are consistent with the better C_2H_6-selectivity for Cu-MOF(NH_2) than Cu-MOF, as found in experimental results.

Furthermore, the more different binding sites were further explored by GCMC simulations at 298 K and 100 kPa to evaluate the binding of C_2H_4 and C_2H_6 molecules in Cu-MOF (Fig. 7) and Cu-MOF(NH_2) (Fig. 8). The detailed data on these interactions was listed in Table S4. The results revealed that the adsorption sites are mainly located in cavities for two MOFs through forming C–H···C/N/O/π interactions. Comparing the interactions between the framework and gas molecules: C_2H_4 in Figs. 7a and b *vs.* C_2H_6 in Figs. 7c and d for Cu-MOF; C_2H_4 in Figs. 8a and b *vs.* C_2H_6 in Figs. 8c and d for Cu-MOF(NH_2), it clearly revealed that the interactions between the framework and C_2H_6 are more and stronger than C_2H_4 in two MOFs. In particular, the -NH_2 groups in Cu-MOF(NH_2) make both C_2H_6 and C_2H_4 molecules have closer contacts with the framework, leading to increased C–H···N interactions as a result, and which is more evident for C_2H_6 in pores, agreeing well with the experimental findings of more C_2H_6 capture and higher C_2H_6/C_2H_4 selectivity in Cu-MOF(NH_2) relative to Cu-MOF.

In summary, based on pore decoration strategy, we have effectively tuned the pore environment through installing -NH_2 functionalized groups and obtained an isomorphic Cu-MOF(NH_2) for targeting highly efficient one-step C_2H_4 purification from C_2H_6/C_2H_4 mixtures. The -NH_2 groups enhanced the interactions of the framework with C_2H_6 molecules, which preferentially adsorbed more C_2H_6 from C_2H_6/C_2H_4 mixtures. Cu-MOF(NH_2) with high C_2H_6 uptakes and significant C_2H_6/C_2H_4 selectivity effectively reduced "trade-off" effect in comparison to Cu-MOF. As a result, Cu-MOF(NH_2) produced polymer-grade C_2H_4 (≥99.99%) in one-step separation with a high productivity of 30.02 L/kg, which was 3.3 times higher than that of C_2H_4 produced by Cu-MOF, and a significantly higher purity than Cu-MOF. The utilization of this pore engineering approach will aid in the development and utilization of MOF materials for the challenging separation of critical chemicals.

Declaration of competing interest

The authors declare that they have no known competing financial interests or personal relationships that could have appeared to influence the work reported in this paper.

Acknowledgments

This work is supported by National Natural Science Foundation of China (Nos. 22371226 and 22371225) and Natural Science Basic Research Program of Shaanxi (No. 2024JC-JCQN-18).

Supplementary materials

Supplementary material associated with this article can be found, in the online version, at doi:10.1016/j.cclet.2024.109729.

References

[1] S.M. Sadrameli, Fuel 173 (2016) 285–297.
[2] R. Sahoo, M.C. Das, Coord. Chem. Rev. 442 (2021) 213998.
[3] D.S. Sholl, R.P. Lively, Nature 532 (2016) 435–437.
[4] S. Chu, Y. Cui, N. Liu, Nat. Mater. 16 (2016) 16–22.
[5] J.Y. Li, Y. He, Y.C. Zou, et al., Chin. Chem. Lett. 33 (2022) 3017–3020.
[6] P.Q. Liao, N.Y. Huang, W.X. Zhang, et al., Science 356 (2017) 1193–1196.
[7] H. Zeng, M. Xie, T. Wang, et al., Nature 595 (2021) 542–548.
[8] X.B. Mu, Y.Y. Xue, M.C. Hu, et al., Chin. Chem. Lett. 34 (2023) 107296.
[9] S. Zhou, O. Shekhah, A. Ramírez, et al., Nature 606 (2022) 706–712.
[10] F. Xie, H. Wang, J. Li, J. Mater. Chem. A 11 (2023) 12425–12433.
[11] F. Zhang, H. Shang, B. Zhai, et al., Angew. Chem. Int. Ed. 62 (2023) e202316149.
[12] M.-H. Yu, H. Fang, H.-L. Huang, et al., Small 19 (2023) 2300821.
[13] S. Mukherjee, D. Sensharma, K.J. Chen, et al., Chem. Commun. 56 (2020) 10419–10441.
[14] C.X. Chen, Z.W. Wei, T. Pham, et al., Angew. Chem. Int. Ed. 60 (2021) 9680–9685.
[15] R.B. Lin, Z. Zhang, B. Chen, Acc. Chem. Res. 54 (2021) 3362–3376.
[16] H. Wang, D. Luo, E. Velasco, et al., J. Mater. Chem. A 9 (2021) 20874–20896.
[17] G.D. Wang, R. Krishna, Y.Z. Li, et al., Angew. Chem. Int. Ed. 61 (2022) e202213015.
[18] S. Aguado, G. Bergeret, C. Daniel, et al., J. Am. Chem. Soc. 134 (2012) 14635–14637.
[19] B. Li, Y. Zhang, R. Krishna, et al., J. Am. Chem. Soc. 136 (2014) 8654–8660.
[20] J.E. Bachman, M.T. Kapelewski, D.A. Reed, et al., J. Am. Chem. Soc. 139 (2017) 15363–15370.
[21] Z. Bao, J. Wang, Z. Zhang, et al., Angew. Chem. Int. Ed. 57 (2018) 16020–16025.
[22] R.B. Lin, L. Li, H.L. Zhou, et al., Nat. Mater. 17 (2018) 1128–1133.
[23] L. Zhang, L. Li, E. Hu, et al., Adv. Sci. 7 (2019) 1901918.
[24] L. Li, R.B. Lin, R. Krishna, et al., Science 362 (2018) 443–446.
[25] Z. Xu, X. Xiong, J. Xiong, et al., Nat. Commun. 11 (2020) 3163.
[26] Y. Wang, C. Hao, W. Fan, et al., Angew. Chem. Int. Ed. 60 (2021) 11350–11358.
[27] G.D. Wang, Y.Z. Li, W.J. Shi, et al., Angew. Chem. Int. Ed. 61 (2022) e202205427.
[28] H. Sun, F. Chen, R. Chen, et al., Small 19 (2023) 2208182.
[29] W. Liang, Y. Wu, H. Xiao, et al., AIChE J. 64 (2018) 3390–3399.
[30] H.G. Hao, Y.F. Zhao, D.M. Chen, et al., Angew. Chem. Int. Ed. 57 (2018) 16067–16071.

[31] O.T. Qazvini, R. Babarao, Z.L. Shi, et al., J. Am. Chem. Soc. 141 (2019) 5014–5020.
[32] H. Zeng, X.J. Xie, M. Xie, et al., J. Am. Chem. Soc. 141 (2019) 20390–20396.
[33] J. Pei, J.X. Wang, K. Shao, et al., J. Mater. Chem. A 8 (2020) 3613–3620.
[34] X.J. Xie, H. Zeng, W. Lu, et al., J. Mater. Chem. A 11 (2023) 20459–20469.
[35] Y. Ye, Y. Xie, Y. Shi, et al., Angew. Chem. Int. Ed. 62 (2023) e202302564.
[36] S.Q. Yang, T.L. Hu, Coord. Chem. Rev. 468 (2022) 214628.
[37] J.R. Li, R.J. Kuppler, H.C. Zhou, Chem. Soc. Rev. 38 (2009) 1477–1504.
[38] P.Q. Liao, W.X. Zhang, J.P. Zhang, et al., Nat. Commun. 6 (2015) 8697.
[39] R.B. Lin, H. Wu, L. Li, et al., J. Am. Chem. Soc. 140 (2018) 12940–12946.
[40] K.J. Chen, D.G. Madden, S. Mukherjee, et al., Science 366 (2019) 241–246.
[41] J. Liu, J. Miao, H. Wang, et al., AIChE J. 69 (2023) e18021.
[42] S.M. Wang, H.R. Liu, S.T. Zheng, et al., Sep. Purif. Technol. 304 (2023) 122378.
[43] X. Lin, Y. Yang, X. Wang, et al., Sep. Purif. Technol. 330 (2024) 125252.
[44] K. Zhang, F. Chu, Y. Hu, et al., Chin. Chem. Lett. 34 (2023) 107766.
[45] H. Yang, Y. Wang, R. Krishna, et al., J. Am. Chem. Soc. 142 (2020) 2222–2227.
[46] U. Böhme, B. Barth, C. Paula, et al., Langmuir 29 (2013) 8592–8600.
[47] Y. Chen, Z. Qiao, H. Wu, et al., Chem. Eng. Sci. 175 (2018) 110–117.
[48] W. Liang, F. Xu, X. Zhou, et al., Chem. Eng. Sci. 148 (2016) 275–281.
[49] R. Krishna, ACS Omega 5 (2020) 16987–17004.
[50] X.W. Gu, J.X. Wang, E. Wu, et al., J. Am. Chem. Soc. 144 (2022) 2614–2623.